PCCP

ROYAL SOCIETY OF CHEMISTRY

PAPER

View Article Online
View Journal | View Issue

Cite this: *Phys. Chem. Chem. Phys.*, 2022, **24**, 18291

In silico binding affinity prediction for metabotropic glutamate receptors using both endpoint free energy methods and a machine learning-based scoring function†

Jingchen Zhai,[a] Xibing He,[a] Yuchen Sun,[a] Zhuoya Wan,[b] Beihong Ji,[a] Shuhan Liu,[a] Song Li[b] and Junmei Wang *[a]

Received 14th April 2022,
Accepted 12th July 2022

DOI: 10.1039/d2cp01727j

rsc.li/pccp

Metabotropic glutamate receptors (mGluRs) play an important role in regulating glutamate signal pathways, which are involved in neuropathy and periphery homeostasis. mGluR4, which belongs to Group III mGluRs, is most widely distributed in the periphery among all the mGluRs. It has been proved that the regulation of this receptor is involved in diabetes, colorectal carcinoma and many other diseases. However, the application of structure-based drug design to identify small molecules to regulate the mGluR4 receptor is limited due to the absence of a resolved mGluR4 protein structure. In this work, we first built a homology model of mGluR4 based on a crystal structure of mGluR8, and then conducted hierarchical virtual screening (HVS) to identify possible active ligands for mGluR4. The HVS protocol consists of three hierarchical filters including Glide docking, molecular dynamic (MD) simulation and binding free energy calculation. We successfully prioritized active ligands of mGluR4 from a set of screening compounds using HVS. The predicted active ligands based on binding affinities can almost cover all the experiment-determined active ligands, with only one ligand missed. The correlation between the measured and predicted binding affinities is significantly improved for the MM-PB/GBSA-WSAS methods compared to the Glide docking method. More importantly, we have identified hotspots for ligand binding, and we found that SER157 and GLY158 tend to contribute to the selectivity of mGluR4 ligands, while ALA154 and ALA155 could account for the ligand selectivity to mGluR8. We also recognized other 5 key residues that are critical for ligand potency. The difference of the binding profiles between mGluR4 and mGluR8 can guide us to develop more potent and selective modulators. Moreover, we evaluated the performance of IPSF, a novel type of scoring function trained by a machine learning algorithm on residue–ligand interaction profiles, in guiding drug lead optimization. The cross-validation root-mean-square errors (RMSEs) are much smaller than those by the endpoint methods, and the correlation coefficients are comparable to the best endpoint methods for both mGluRs. Thus, machine learning-based IPSF can be applied to guide lead optimization, albeit the total number of actives/inactives are not big, a typical scenario in drug discovery projects.

Introduction

G-protein coupled receptor (GPCR) is a major therapeutic drug target class in today's drug discovery and development. Metabotropic glutamate receptors (mGluRs),[1–4] which belong to the Class C GPCRs, are widely distributed in both the central nervous system and the periphery.[5] The mGluRs have been considered as predominant mediators of glutamatergic signaling in many cancers, and the abnormal expression level of mGluRs contributes to many diseases,[6] including Parkinson's disease, Alzheimer's disease and other brain disorder diseases.[7,8] There are three subgroups of mGluRs, termed Group I (mGluR1 and mGluR5), Group II (mGluR2 and nGluR3), and Group III (mGluR4,

[a] *Department of Pharmaceutical Sciences and Computational Chemical Genomics Screening Center, School of Pharmacy, University of Pittsburgh, Pittsburgh, PA 15261, USA. E-mail: junmei.wang@pitt.edu*
[b] *Department of Pharmaceutical Sciences and Center for Pharmacogenetics, School of Pharmacy, University of Pittsburgh, Pittsburgh, PA 15261, USA*

† Electronic supplementary information (ESI) available: Information of available crystal structures and experiment Ki binding data of mGluR proteins is shown in Table S1. Detailed MM-PB/GBSA binding free energies of each ligand-receptor system are shown in Tables S2–S9. A sequence comparison between mGluR4 and mGluR8 is shown in Fig. S1. Fluctuation of root-mean-square-deviations along the time course of MD simulations for representative systems are shown in Fig. S2–S5. See DOI: https://doi.org/10.1039/d2cp01727j

mGluR6, mGluR7, and mGluR8).[9] Among all the mGluRs,[5] mGluR4 is the most widely expressed in the periphery while both the inhibition and the activation of this receptor can trigger therapeutic effects. For example, the activation of mGluR4 may reduce glucagon production for patients with diabetes and reduce cell proliferation in medulloblastoma conditions,[9,10] whereas the inhibition of mGluR4 receptors can decrease cell survival and invasiveness as well as improve response to other chemotherapies for patients with colorectal carcinoma.[11,12] Growing evidence has shown that the regulation of mGluR4 is of great therapeutic interest.[1,4–6,13–15] However, our availability of the active ligands targeting mGluR4 is relatively limited due to many factors including the absence of a resolved mGluR4 protein structure. The availability of experimental structures for mGLURs is summarized in Table S1 (ESI†).

Computer-aided drug design (CADD) has exerted great influence as technologies evolve. Among the widely used CADD methods, some possess the advantages of high efficiency, such as molecular docking, and some can predict protein–ligand binding affinity with high accuracies, such as the free energy-based methods in conjunction with molecular dynamics (MD) simulation. Thus, employing different types of scoring functions for virtual screening in a hierarchical way can greatly balance computational efficiency and accuracy. Our hierarchical virtual screening (HVS) scheme consists of two types of scoring functions. First of all, Glide docking,[16] a popular molecular docking program implemented in the Schrodinger software package, is utilized to screen a large compound library effectively. After the tree is pruned, the hits of docking screening are further prioritized by the MM-PB/GBSA (molecular mechanics Poisson–Boltzmann/Generalized Born surface area) filter.[17,18] Prior to the MM-PB/GBSA free energy calculation, MD simulation is usually performed to confirm the stability of protein–ligand binding and to sample the conformations of a ligand residing in the binding pocket of the drug target. The MD simulation step is necessary when a ligand binding triggers a significant conformational change. In this study, we conducted an HVS study for mGluR4 using a compound library with various measured activities. A homology modeling technique will be first utilized to build the structural model of mGluR4 with a crystal structure of mGluR8 as the template. Recently, the structure of mGluR4 has been published for the first time with a resolution of 4.00 Å (PDB ID: 7E9H).[19] The structure difference between the published one and the one we built reports a root-mean-square-deviation (RMSD) value of 2.03 Å (435 residues aligned and 3304 atoms compared). The small RMSD value indicates the reliability of our homology modeling result. Besides the endpoint MM-PBSA-WSAS and MM-GBSA-WSAS methods, we will explore the possibility of applying interaction profile scoring function (IPSF),[20] recently developed by us in a drug lead optimization procedure for a typical drug target. IPSF has been successfully applied in a drug lead identification procedure for multiple drug targets.[20] The findings of this work will not only facilitate the discovery of novel inhibitors selectively targeting an mGLUR by providing the structures of receptors and an adequate screening protocol, but also demonstrate the potential of applying IPSF in drug lead optimization.

Method

Homology modeling

Both mGluR7 and mGluR8 in the group III mGluRs have available crystal structures, which might be adopted as a template for building a homology model of mGluR4. However, so far in the ChEMBL database (**https://www.ebi.ac.uk/chembl/**, accessed on 08/01/2020) there is only one ligand with the reported K_i value $<100\,000$ nM targeting mGluR7.[21] On the contrary, the mGLuR8 protein has a series of ligands with the K_i values ranging from 61 nM to over 300 000 nM. Given the fact that mGluR4 shares 78.98% secondary structure similarity with mGluR8 (Fig. S1, ESI†), it is expected that a high-quality homology model of mGluR4 can be generated using the mGluR8 structure as a template. The protein sequence of mGluR4 was downloaded from Uniprot (**https://www.uniprot.org**) and sequence alignment between mGluR4 and mGluR8 was conducted using the PROMALS3D webserver (**https://prodata.swmed.edu/promals3d/promals3d.php**).[22,23] After a crystal structure of mGluR8 (PDBID: 6BT5, resolution: 2.92 Å) was downloaded from the Protein Data Bank (**https://www.rcsb.org/**),[24] we used Modeller 9.20 to build the homology model of mGluR4 in this study.[25,26] Among the 1000 homology models of mGluR4 generated by Modeller, both the discrete optimized protein energy (DOPE) scores and the main chain root-mean-square deviations (RMSDs) between the template and models were taken into consideration to select a set of top models.[27] Among these top-ranked models, the homology model in which the experimental binding free energies and Glide docking scores of mGluR4 ligands had the best correlation was selected for further studies.[28,29]

Molecular docking

Molecular docking was performed to preliminarily identify high-affinity ligands from a compound library. The flexible-ligand docking simulations were performed using the Glide docking module in the Schrodinger software suite with the standard precision (SP) version of the Glide docking scoring function.[28] The correlation between the predicted docking scores and the experimental binding affinities for the ligands being successfully docked to the binding pocket is utilized to evaluate the performance of the scoring function in docking screening. The experimental binding free energy $\Delta G_{binding}$ is converted from reported K_i data according to the following equation:

$$\Delta G_{binding} = -RT \ln K_i \quad (1)$$

where R is the gas constant (8.314 J mol^{-1} K^{-1}) and T is the room temperature with the value of 298.15 K. We first downloaded all the ligands for both mGlurR4 and mGluR8 from the ChEMBL database and built the ligand libraries for each receptor, respectively. The Ligprep module of the Schrodinger software (Maestro version 11.2)[30] was utilized for ligand preparation: generating possible ligand states at target pH ranging from 5.0 to 9.0, determining chirality from the 3D structure, and writing out at most 32 states per ligand. Next, we used the

Protein Preparation Wizard module to prepare protein receptors with default settings including hydrogen adding, water and co-crystallized solvents removing, and energy minimization for hydrogen atoms of the receptors. The selected top-ranked mGluR4 homology models and mGluR8 crystal structure were prepared at this step. The refined mGlur4 models were aligned to the refined mGluR8 model so that the binding pockets of both receptors are well overlapped. For each receptor, the grid file was generated using the Receptor Grid Generation module with the center of the binding grid being located at the geometric center of the co-crystallized binding ligand (Residue Name E7P) of mGluR8 and the default values of other parameters being kept unchanged. There were no other constraints and rotatable groups defined at this step. Flexible docking simulation was performed with the Glide Docking module, with the scaling factor of van der Waals radius and partial charge cutoff value of 0.80 and 0.15, respectively, and intramolecular hydrogen bonds being rewarded. At most 10 poses per ligand were written out. For each compound, the docking pose with the best docking score was selected to enter the next stage of HVS.

System setup for MD simulations

Because our flexible docking method only calculates the docking score of a ligand to a static receptor, we conducted MD simulations to study the conformational change of the receptor triggered by ligand binding. The collected MD snapshots were then applied to calculate the protein–ligand binding free energy using an endpoint method. MD simulation is a method to mimic the dynamics of ligand binding under the sub-cellular environment. For this reason, the prediction results of MD simulation, which were reflected by the calculated binding free energy values, are closer to the real state. During the MD simulation process, the protein–ligand complexes are immersed in the NaCl solvent and finally come to a dynamic balance governed by the AMBER forcefields.

Each MD system consists of one copy of the mGluR4 or mGluR8 receptor and one docked ligand within a rectangular box with approximately 9000 TIP3P water molecules and about 50 Na^+ and Cl^- ions depending on the charge state of the ligand.[31] The whole system was neutralized. The starting conformation of the ligand in the corresponding receptor–ligand complex was from the selected best docking pose. For the force field parameters, the partial atomic charges of ligands were derived using the RESP program to fit the HF/6-31G* electrostatic potentials generated using the Gaussian 16 software package,[32,33] and the other force field parameters for ligands is the General Amber force field (GAFF) in AMBER 18.[34,35] The Antechamber module was utilized to generate residue topologies of ligands.[36] The AMBER FF14SB force field was employed to model protein receptors.[37]

Molecular dynamics (MD) simulations

MD simulations were performed to produce isothermal–isobaric ensembles by the PMEMD.mpi and PMEMD.cuda modules in the AMBER 18 package.[31] The pressure was set to 1 atm, regulated by the Berendsen barostat.[38] Five steps of energy minimization were performed with the mainchain atoms of the receptor and the bound ligand being restrained, using the harmonic restraint force constraints decreased from 20 to 10, 5, 1, and finally 0 kcal mol^{-1} $Å^{-2}$ progressively. After minimizations, the temperature of each system was heated from 50 K to 298.15 K within 3 ns, and then kept at 298.15 K, which was regulated by Langevin dynamics with a collision frequency of 5 ps^{-1},[39] to simulate the physiological environment. After undergoing the equilibrium phase for 50 ns, each system kept running MD simulation for another 150 ns for sampling. In total, a 203 ns MD simulation was performed on each ligand with a time step of 2 fs. The trajectories were saved every 10 ps for post-analysis, including the calculations of MM-PB/GBSA binding free energy and root-mean-square deviation (RMSD) fluctuations of ligands and receptors.

MM-PB/GBSA binding free energy calculations

Molecular mechanics-Poisson Boltzmann/Generalized Born surface area (MM-PB/GBSA) is a widely used endpoint method in solvent binding free energy calculations.[39–46] In this study, the MM-PB/GBSA binding free energy of each ligand was calculated with the following equations:

$$\Delta G_{\text{MM-PB/GBSA}} = \Delta H - T\Delta S = \Delta E_{\text{MM}} + \Delta G_{\text{sol}} - T\Delta S \quad (2)$$

$$\Delta E_{\text{MM}} = \Delta E_{\text{vdw}} + \Delta E_{\text{ele}} + \Delta E_{\text{inter}} \quad (3)$$

$$\Delta G_{\text{sol}} = \Delta G_{\text{p}}^{\text{sol}} + \Delta G_{\text{np}}^{\text{sol}} \quad (4)$$

where ΔE_{vdw} and ΔE_{ele} are the changes of van der Waals energy and electrostatic energy, respectively. ΔE_{inter} is the change of internal energy (bond, angle, and dihedral energies) upon ligand binding. The gas phase MM energy change, ΔE_{MM}, is the sum of the above three energy terms. ΔG_{sol}, the solvation free energy, is the sum of electrostatic solvation energy $\Delta G_{\text{p}}^{\text{sol}}$ and the non-electrostatic solvation energy $\Delta G_{\text{np}}^{\text{sol}}$. $\Delta G_{\text{p}}^{\text{sol}}$, the polar component of solvation free energy, is calculated by solving the Poisson Boltzmann or the Generalized Born equations. $\Delta G_{\text{np}}^{\text{sol}}$, the nonpolar component of the solvation free energy is usually estimated using the solvent-accessible surface area (SASA). $T\Delta S$, the change of entropy upon ligand binding, can be predicted by normal mode analysis. However, in this work, we applied a weighted solvent accessible surface (WSAS) model to estimate the ΔS term.[43] As such, this free energy method is called MM-PB/GBSA-WSAS. The contribution from internal energies ΔE_{inter} cancels out in the "Single Trajectory" protocol,[40,47] and the ΔE_{vdw}, ΔE_{ele}, and $T\Delta S$ are the same in MM-PBSA and MM-GBSA binding free energy calculation.

$$\Delta G_{\text{MM-PB/GBSA}} = \Delta E_{\text{vdw}} + \Delta E_{\text{ele}} + \Delta G_{\text{p}}^{\text{sol}} + \Delta G_{\text{np}}^{\text{sol}} - T\Delta S \quad (5)$$

450 snapshots were evenly collected from the MD sampling phase of each system for the subsequent MM-PB/GBSA binding free energy calculation.

Machine learning (ML)-based IPSF scoring functions

To develop interaction profile (IP) based scoring functions, the first step is to accurately calculate the ligand–residue interaction energies. We calculated the MM-GBSA free energies between the ligand and all receptor residues for 4000 snapshots collected in the sampling phase of MD simulations. An internal program was applied to analyze the outputs of Sander decomposition jobs and conduct statistical analysis on each component of the MM-GBSA free energy. The regression learner module in the MATLAB software (version R2020b) was used for constructing regression models. The applied ML algorithms include linear regression models, regression trees, support vector machines (SVM), Gaussian process regression models, and ensembles of trees. Five-fold validation and ten-fold validation were both considered with or without principal component analysis (PCA) of IP data. For PCA, two modes were investigated, one set the explained variance to be 95%, the other explicitly specified the number of principal components, X, where X ranged from 1 to 5.

Results and discussion

1 Molecular docking and MD simulation of mGluR8

The molecular docking result of mGlur8 showed a weak correlation between the docking score and the experimental ΔG. We first evaluated the practicability of a crystal structure of mGluR8 in a VHS study, as this structure was applied by us to construct the homology models of mGluR4. To uncover the preliminary correlation between the experimental ΔG and predicted binding affinity using the Glide docking scoring function for mGluR8 and its ligands, we built the ligand library of mGlur8 consisting of 20 ligands, which include all available compounds from the ChEMBL database with reported experimental K_i values (Table S1, ESI†). The experimental ΔG calculated from the reported K_i value and the docking score of each ligand in the library docked to the mGlur8 receptor are listed in Table 1. The correlation between docking scores and experimental ΔG of ligands is shown in Fig. 1(A), with a correlation coefficient R of 0.30. Interestingly, there were 2 ligands, CHEMBL39338 and CHEMBL40123, that achieved very low docking scores, which mean a high predicted binding affinity, and actually had rather large K_i values (low experimental binding affinity). Both compounds possess benzene rings in their chemical structures. After excluding these two ligands, the R-value was increased to 0.45. This phenomenon further showed the lower accuracy of the molecular docking method in ligand–protein affinity prediction. Nevertheless, molecular docking is an efficient screening method and is suitable for screening large compound libraries at the early stage of VHS. All the 20 ligands for mGluR8 in the library were further evaluated using the following more accurate screening filters.

MD simulations and MM-PB/GBSA-WSAS binding free energy calculation for mGluR8 showed an elevated correlation with the experimental ΔG. The RMSDs of the ligand and the mGluR8 receptor during the simulation process are shown in Fig. S2, S3 (ESI†), and the predicted binding free energy by different PB or GB models of each ligand is listed in Table 1. The 7 experimental top-ranked ligands (experimental K_i < 10 000 nM, $\Delta G < -6.8$ kcal mol^{-1}) were considered as active ligands, whereas the rest of the ligands with K_i equal to or larger than 10 000 nM were regarded as inactive ones. Six out of the 7 active ligands were predicted to have very low binding free energy (thus high binding affinity) during MM-PB/GBSA binding free energy calculation under different PG/GB models except for CHEMBL277475. The binding stability of a ligand is evaluated using the time courses of root-mean-square

Table 1 The list of ligand experimental binding free energies, glide docking scores and MM-PB/GBSA-WSAS binding free energies (in kcal mol^{-1}) for ligands binding to mGlur8 receptor. The R-value reflects the correlation between experimental binding free energies and glide docking score or MM-PB/GBSA-WSAS binding free energies for ligands

Molecule ID	$\Delta G_{\text{Experimental}}$	Docking score	$\Delta G_{\text{MM-GBSA1}}$	$\Delta G_{\text{MM-GBSA2}}$	$\Delta G_{\text{MM-GBSA5}}$	$\Delta G_{\text{MM-PBSA}}$
CHEMBL33567	−9.81	−7.34	−81.95	−83.01	−100.89	−33.35
CHEMBL432038	−9.21	−5.51	−67.80	−60.50	−53.64	−16.02
CHEMBL277475	−9.08	−7.47	−24.88	−10.12	−2.17	11.55
CHEMBL275079	−7.85	−8.27	−67.10	−66.43	−82.01	−30.84
CHEMBL280563	−7.44	−6.77	−60.91	−61.12	−85.62	−27.01
CHEMBL88999	−6.99	−7.52	−61.79	−53.28	−54.21	−27.16
CHEMBL575060	−6.83	−6.36	−73.93	−69.41	−83.83	−34.36
CHEMBL229429	−6.80	−5.79	0.02	4.10	12.33	3.41
CHEMBL1672288	−6.80	−5.82	−9.21	0.05	16.72	14.73
CHEMBL8759	−6.69	−7.56	−60.66	−47.40	−35.63	−26.59
CHEMBL330097	−6.56	−7.63	−51.52	−31.79	5.74	−16.20
CHEMBL34453	−5.91	−7.53	−45.33	−18.53	5.58	−13.41
CHEMBL40086	−5.44	−7.24	−18.33	6.61	54.82	18.49
CHEMBL327783	−5.44	−4.96	−5.67	−0.10	13.38	2.62
CHEMBL66654	−5.44	−4.25	−14.76	−7.84	6.35	6.96
CHEMBL88553	−5.44	−4.54	7.04	8.49	10.14	9.40
CHEMBL88612	−5.44	−3.96	−9.21	−4.52	9.02	10.63
CHEMBL39338	−4.79	−7.18	−63.94	−45.67	−42.88	−11.98
CHEMBL40123	−4.79	−7.61	−27.52	−11.02	16.24	8.59
CHEMBL39221	−4.08	−5.83	53.16	68.96	96.42	102.86
R	—	0.30	0.60	0.66	0.67	0.55

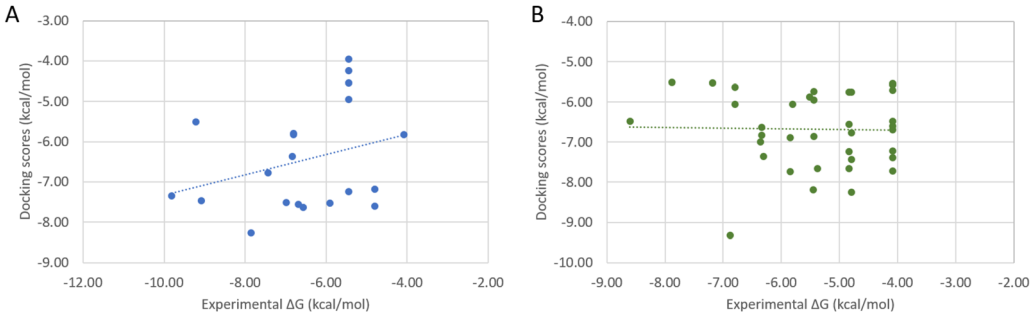

Fig. 1 The correlation analysis between experimental ligand-binding affinities and docking scores for mGluR8 (A) and mGluR4 (B) receptors.

deviations (RMSDs) in MD simulations for atom subsets including mainchain atoms of the receptor, the ligand w/wo least-square fittings. To calculate the RMSD of a ligand without least-square fitting, we first conducted the least-square fitting for the main chain atoms of the receptor, and the resulting translation and rotation matrixes were applied to the ligand, and the RMSD was calculated directly. As such, a No-Fit RMSDs measure not only the conformational change of a ligand, but its translational and rotational movement in the binding pocket. All the 6 active ligands had all types of RMSDs smaller than 6 Å and came to a stable state for at least half of the simulation time. The small fluctuation of the RMSDs of the active ligands demonstrates the stable binding of the ligands to their receptor protein. Among those considered inactive ligands, some of them tended to have extremely unstable binding conformations in the binding pocket, thus caused very large RMSD fluctuation. In an extreme scenario, some inactive ligands which include CHEMBL1672288 and CHEMBL88553 even drifted out of the protein binding site, leading to extremely large values of the ligand's Non-Fit RMSDs. All inactive ligands were predicted to have a higher binding free energy, although some of them may seem to remain stable in the ligand–protein binding complexes, with a lower RMSD fluctuation of each subject, suggesting the MD simulation filter itself cannot screen out all the inactive compounds in HVS.

The last filter in our HVS is endpoint binding free energy calculations. We found that the predicted MM-PBSA-WSAS binding free energies and experimental ΔG of the total 20 ligands showed an improved correlation with R of 0.55, compared to R of 0.3 for the docking screening. Interestingly, all three MM-GBSA-WSAS scoring functions achieved a better correlation than MM-PBSA-WSAS for this system. The correlation coefficients are 0.60, 0.66, and 0.67 for MM-GBSA1 (igb = 1),[48] MM-GBSA2 (igb = 2),[49] and MM-GBSA5 (igb = 5),[49] respectively. The correlation analysis graphs between the predicted *versus* the

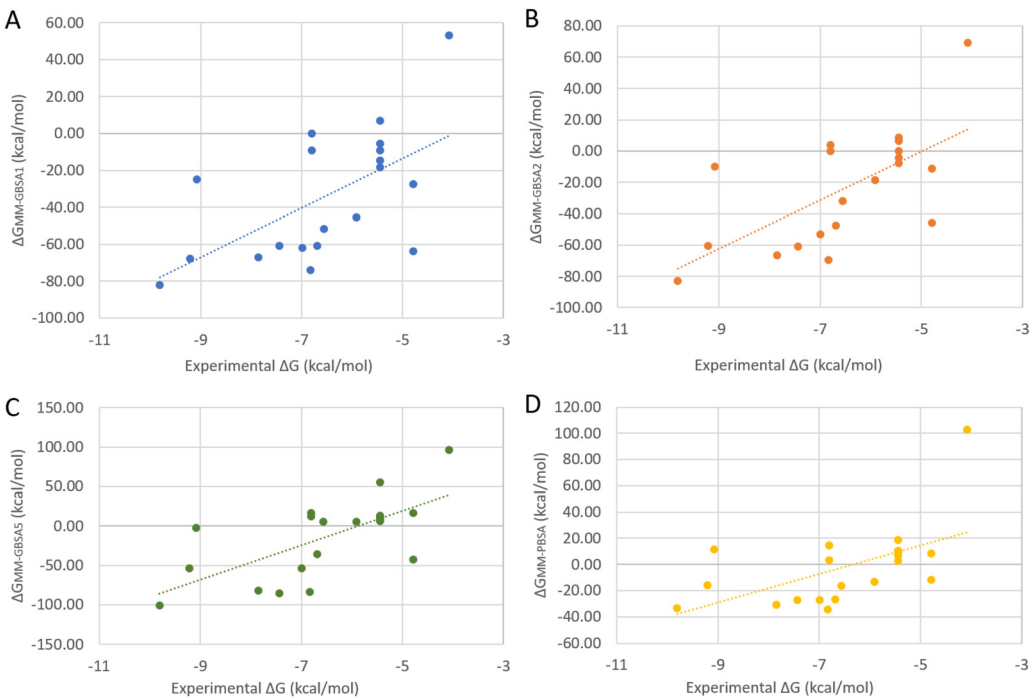

Fig. 2 The correlation between experimental and the predicted binding free energies for mGluR8 ligands using different endpoint models. (A) MM-PBSA, (B) MM-GBSA1, (C) MM-GBSA2, and (D) MM-GBSA5. The entropy contribution ($T\Delta S$) was estimated using the WSAS model.

measured binding affinities for different PB/GB models are shown in Fig. 2. The above results show that our HVS method has a high practicability in identification of active ligands for the mGluR8 structure, thus laying a solid foundation for us to identify active ligands of mGluR4 with a homology model constructed using the mGluR8 structure as the template.

2 Homology modeling, molecular docking and MD simulation for mGluR4

Evaluation of homology models of mGluR4 and selection of ligands for the subsequent VHS study. We collected 76 ligands from the CHEMBL website to build the library of mGluR4 ligands. Among the 1000 homology models generated for mGluR4, three models with the best DOPE scores, three models with the smallest RMSDs and three models with both top-ranking DOPE and RMSE scores were selected as top-ranked models. Among these nine models, the one leading to the best correlation between predicted docking scores and experimental ΔG of the mGluR4 ligand library (R = 0.15) was selected for the subsequent study. For this selected mGluR4 model, we ranked the ligands by their docking score from low to high, and selected the first half which includes most of the real active ligands for further MD simulation experiments. This kind of strategy is commonly adopted in real scenarios of virtue screening, *i.e.*, selecting top-ranked ligands from docking for further studies, either experimental measurement or virtual screening by more accurate CCAD methods. The R value between the measured binding affinities and docking scores of the selected ligands is only 0.02 (Fig. 1(B)), suggesting more accurate methods are needed to discriminate those ligands.

MD simulation results and MM-PB/GBSA-WSAS binding free energy calculation results for mGluR4. The plots of the RMSD time courses for every ligand binding to mGluR4 protein are shown in Fig. S4 and S5 (ESI†). It is observed that all 29 ligands have RMSD values lower than 6 Å, the cutoff (Fig. S4, ESI†), while 8 ligands have some values of their No-Fit ligand RMSDs larger than the cutoff (Fig. S5, ESI†). All ligands with reported K_i values larger than 10 000 nM were considered as inactive ligands. All the four experimental top-ranked ligands with K_i values smaller than 10 000 nM ($\Delta G < -6.80$ kcal mol^{-1}, considered as active ligands) have only mild RMSD fluctuations and the predicted MM-PBSA binding free energies are very low,

Table 2 The list of ligand experimental binding free energies, glide docking scores, and MM-PB/GBSA binding free energies (in kcal mol^{-1}) for ligands binding to the mGlur4 homology model. The R-value reflects the correlation between experimental binding free energies and glide docking scores or MM-PB/GBSA binding free energies for ligands

Molecule ID	$\Delta G_{\text{Experimental}}$	Docking score	$\Delta G_{\text{MM-GBSA1}}$	$\Delta G_{\text{MM-GBSA2}}$	$\Delta G_{\text{MM-GBSA5}}$	$\Delta G_{\text{MM-PBSA}}$
CHEMBL33567	−8.61	−6.48	−79.18	−93.17	−123.59	−37.85
CHEMBL575060	−7.88	−5.51	−59.43	−48.42	−37.11	−21.43
CHEMBL277475	−7.19	−5.52	−37.47	−23.32	−14.03	−1.12
CHEMBL329236	−6.88	−9.32	−66.73	−58.31	−53.19	−23.57
CHEMBL229429	−6.80	−6.06	−12.75	−1.94	20.44	8.47
CHEMBL1672288	−6.80	−5.64	−12.83	−3.74	14.48	7.47
CHEMBL275079	−6.36	−6.99	−62.95	−52.81	−47.62	−26.09
CHEMBL432038	−6.33	−6.82	−71.52	−61.55	−50.90	−17.90
CHEMBL330097	−6.33	−6.64	−8.55	3.29	34.94	5.68
CHEMBL90501	−6.31	−7.36	−65.29	−47.04	−39.49	−24.53
CHEMBL39573	−5.85	−7.73	−71.77	−71.12	−84.86	−29.14
CHEMBL280563	−5.85	−6.88	−29.72	−24.40	−8.40	−1.02
CHEMBL230951	−5.81	−6.06	−69.14	−77.99	−104.51	−28.18
CHEMBL279838	−5.52	−5.88	−69.69	−40.08	1.77	−7.02
CHEMBL34453	−5.45	−8.18	−60.06	−38.31	−26.28	−23.39
CHEMBL8759	−5.44	−6.86	−65.55	−57.85	−64.99	−28.72
CHEMBL327783	−5.44	−5.74	−8.45	11.11	51.74	8.82
CHEMBL305406	−5.44	−5.96	−19.39	1.84	46.32	10.62
CHEMBL279956	−5.37	−7.66	−23.43	0.61	40.14	1.45
CHEMBL2115159	−4.83	−6.56	−30.64	−20.75	−1.27	4.34
CHEMBL2114110	−4.83	−7.24	−15.57	−12.35	−3.56	4.40
CHEMBL2114109	−4.83	−5.75	−24.48	−16.13	3.35	3.86
CHEMBL2114106	−4.83	−7.66	−24.08	−17.80	−2.94	6.59
CHEMBL40123	−4.79	−6.77	−68.10	−45.38	−16.34	−13.48
CHEMBL40086	−4.79	−8.25	−64.29	−27.04	6.60	−24.07
CHEMBL39338	−4.79	−7.43	−71.09	−66.05	−66.47	−9.04
CHEMBL389558	−4.79	−5.76	−23.13	−28.86	−43.70	5.56
CHEMBL88184	−4.08	−6.49	−38.34	−12.53	23.34	4.64
CHEMBL467234	−4.08	−5.58	−43.37	−15.33	15.91	8.34
CHEMBL448885	−4.08	−5.53	−29.90	−0.29	58.81	2.96
CHEMBL444718	−4.08	−5.56	−20.11	0.00	42.91	0.08
CHEMBL315032	−4.08	−7.21	−36.12	−9.80	32.89	−8.84
CHEMBL313938	−4.08	−6.60	−27.25	−19.07	5.32	−7.80
CHEMBL297150	−4.08	−7.39	−35.88	−6.17	34.77	−7.97
CHEMBL284895	−4.08	−7.72	−30.35	−5.79	34.82	5.41
CHEMBL2021372	−4.08	−5.71	−37.54	−14.91	41.30	−4.71
CHEMBL126608	−4.08	−6.69	−35.63	1.19	55.01	8.36
R	—	0.02	0.31	0.50	0.57	0.45

indicating the predicted high affinities between ligands and the protein. The correlation between predicted MM-PBSA binding free energies and experimental ΔG is higher than that of the docking method, with the R-value equal to 0.45. Meanwhile, the correlation between experimental ΔG and the calculation MM-GBSA binding free energies have R-values of 0.31, 0.50, and 0.57 for MM-GBSA1, MM-GBSA2, and MM-GBSA5 models, respectively. Therefore, all the endpoint MM-PB/GBSA-WSAS models achieved a higher correlation between the experimental and predicted binding affinities compared to the Glide docking scoring function. The predicted binding affinities of ligands using different models are listed in Table 2. It is indicated that the most active ligands which have the lowest measured Ki all have very low predicted binding free energies under different MM-PB/GBSA-WSAS models. The performance of each model revealed by correlation analysis is shown in Fig. 3.

During MM-PB/GBSA-WASA binding energy calculation, we tried different energy scales such as setting the inner dielectric constant up to 4 considering that the binding site can partially be accessed by solvent and some polar residues exist.[41] However, the correlations between predicted MM-PBSA-WSAS binding free energies and experimental ΔG did not have significant improvement compared to the result with the inner dielectric constant equal to 1 for both mGluR8 and mGluR4 receptor–ligand systems. Consequently, we kept the default dielectric constant during binding energy calculation.

3 The performance of IPSF-based scoring functions on predicting binding affinities for mGluR8 and mGluR4 proteins

For one ligand binding to mGluR4 or mGluR8, we calculated its IP descriptor using 4000 snapshots collected during the sampling phase of MD simulations. We then applied the "Regression Learner" module implemented in Matlab to construct regression models. The performances of all regression models to predict ligand binding affinity to the receptors are summarized in Table 3. For mGluR8, all the models which have a reported cross validation R-square equal to or larger than 0.25 are listed in the table. There are a series of models for the mGluR8 protein, including SVM, Gaussian process regression and Linear regression models, appearing in both the five-fold and ten-fold cross-validation categories, which might suggest SVM and Gaussian process are good ML algorithms for this problem. The best-performing model using five-fold cross-validation is a squared exponential Gaussian process regression model without conduction PCA (R-square = 0.63, RMSE = 1.2066 kcal mol^{-1}), while the best-performing model using ten-fold cross-validation is a cubic SVM model with PCA (R-value = 0.63, RMSE = 1.2173 kcal mol^{-1}), with PCA for dimensional reduction (the explained variance is equal to or larger than 95%). However, for the mGluR4 protein, there are only three models with their R-squares equal to or larger than 0.2 combining all the models trained under five-fold and ten-fold cross-validation categories, which are much fewer than the models for mGluR8. Two models are medium Gaussian SVM models and the best model is a boosted tress model (R-square = 0.51, RMSE = 1.0293 kcal mol^{-1}). The reason that mGluR4 protein has fewer predictable models lies in the fact that mGluR4 has more inactive ligands than active ones, leading to the unbalanced training data. With more active ligands identified for mGluR4, it is expected that the model performance can be improved. Overall, for both mGluR8 and mGluR4, the predicted RMSEs of cross-validations are smaller

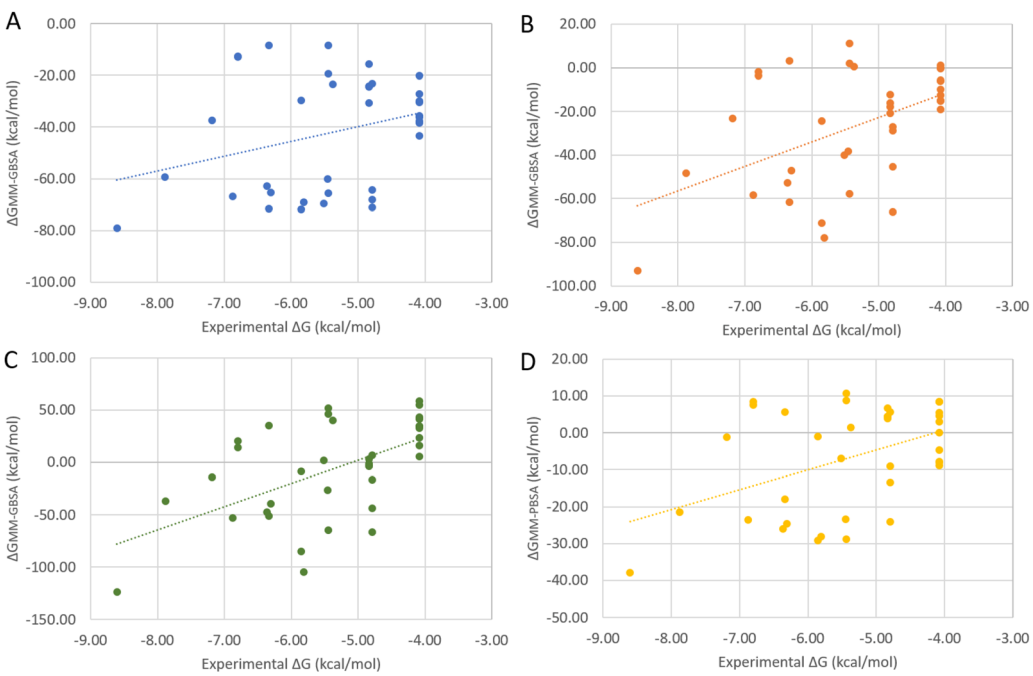

Fig. 3 The correlation between experimental and the predicted binding free energies for mGluR4 ligands using different endpoint models. (A) MM-PBSA, (B) MM-GBSA1, (C) MM-GBSA2, and (D) MM-GBSA5. The entropy contribution ($T\Delta S$) was estimated using the WSAS model.

Table 3 The list of machine-learning trained IPSF models to predict ligand binding activity to mGluR8 and mGluR4 proteins

mGluR8, 5-fold cross validation

PCA	Model type	Model detail	RMSE	*R*-value
Without PCA	SVM	Quadratic SVM	1.2722	0.57
	Gaussian process regression	Squared exponential GPR	1.2066	0.63
PCA (specify explained variance = 95)	Linear regression	Linear	1.2704	0.57
	SVM	Cubic SVM	1.3228	0.53
PCA (specify number of components = 1)	Linear regression	Linear	1.3163	0.53
	SVM	Linear SVM	1.3309	0.52
PCA (specify number of components = 2)	Linear regression	Robust linear	1.3476	0.50
	Stepwise linear regression	Stepwise linear	1.3444	0.50
	SVM	Medium Gaussian SVM	1.2974	0.55
	Gaussian process regression	Squared exponential GPR	1.3473	0.50
	Gaussian process regression	Rational quadratic GPR	1.3473	0.50
PCA (specify number of components = 3)	SVM	Quadratic SVM	1.2711	0.57
PCA (specify number of components = 4)	Linear regression	Linear	1.2463	0.60

mGluR8, 10-fold cross validation

PCA	Model type	Model detail	RMSE	*R*-value
Without PCA	SVM	Cubic SVM	1.3194	0.55
	Gaussian process regression	Squared exponential GPR	1.2814	0.58
PCA (specify explained variance = 95)	SVM	Cubic SVM	1.2173	0.63
PCA (specify number of components = 1)	Linear regression	Linear	1.3472	0.52
	Linear regression	Interactions linear	1.3472	0.52
	Stepwise linear regression	Stepwise linear	1.3472	0.52
	SVM	Linear SVM	1.3608	0.51
	SVM	Coarse Gaussian SVM	1.3585	0.51
PCA (specify number of components = 2)	SVM	Medium Gaussian SVM	1.3528	0.51
	Gaussian process regression	Rational quadratic GPR	1.315	0.55
PCA (specify number of components = 3)	Linear regression	Interactions linear	1.2766	0.58
PCA (specify number of components = 4)	Linear regression	Linear	1.3309	0.54
PCA (specify number of components = 5)	SVM	Cubic SVM	1.2427	0.62

mGluR4, 5-fold cross validation

PCA	Model type	Model detail	RMSE	*R*-value
Without PCA	SVM	Medium Gaussian SVM	1.0749	0.47

mGluR4, 10-fold cross validation

PCA	Model type	Model detail	RMSE	*R*-value
Without PCA	SVM	Medium Gaussian SVM	1.066	0.45
	Ensemble	Boosted trees	1.0293	0.51

than those by MM-PB/GBSA-WSAS, while the correlation coefficients are comparable.

4 The structure–activity relationship of the predicted active ligands for both mGluR8 protein and mGluR4 protein

The predicted ligands with high binding affinities for both mGluR8 and mGluR4 proteins are shown in Fig. 4. Because of the high homology between mGluR8 and mGluR4 proteins, it is not a surprise that some compounds (CHEMBL33567 and CHEMBL575060) are predicted as active ligands for both protein targets. CHEMBL575060 is the glutamic acid, which can be considered as the endogenous ligand of both mGluR8 and mGluR4. Other ligands in Fig. 4 possess structures that are analogous to the glutamic acid, which explains why those compounds have a high predicted binding affinity. To understand the structure–activity relationship (SAR) of these ligands, we collected the representative conformations of these ligands and showed them in Fig. 5. Three aggregations of ligand functional groups in the binding pocket of mGluR8 and mGluR4 proteins can be identified: carboxyl groups ($-COO^-$) and amino groups ($-NH_3^+$) tend to overlap at the left and the top of the binding pocket, and another negatively charged center, represented by functional groups of $-COO^-$, $-SO_3^-$, and $-HPO_3^-$, shows up at the right side of the binding pocket (Fig. 5).

CHEMBL33567, which not only serves as the native ligand of the mGluR8 crystal structure but also is the ligand with the lowest K_i value in our datasets for both mGluR8 and mGluR4. Encouragingly, this compound was predicted as the most active ligand for both receptors under each endpoint free energy model. The reason for the outstanding potency of CHEMBL33567 compared with other glutamic acid analogs can be speculated from Fig. 6 and 7, which show the binding modes of CHEMBL33567 and CHEMBL575060 correspondingly using their representative conformations collected during MD simulation. The representative conformation for a receptor–ligand complex has the lowest

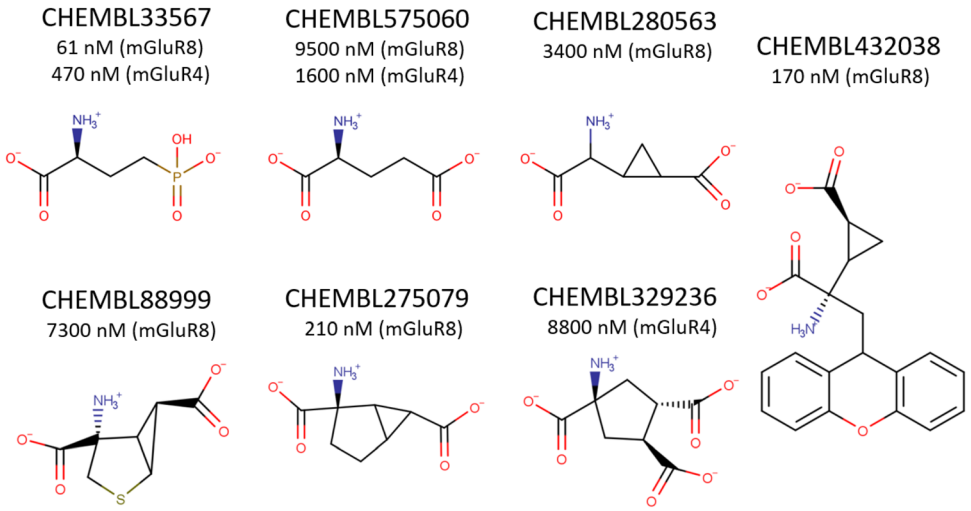

Fig. 4 Predicted active ligands with top-ranking binding affinities for receptor mGluR8 and receptor mGluR4.

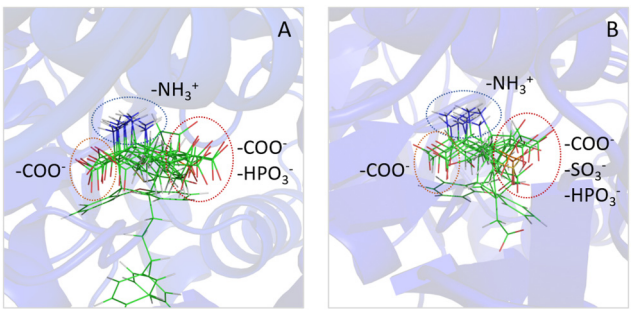

Fig. 5 Functional groups of advantageous ligands from mGluR8 (A) and mGluR4 (B). The binding poses of each ligand are from representative conformations of the collected MD snapshots.

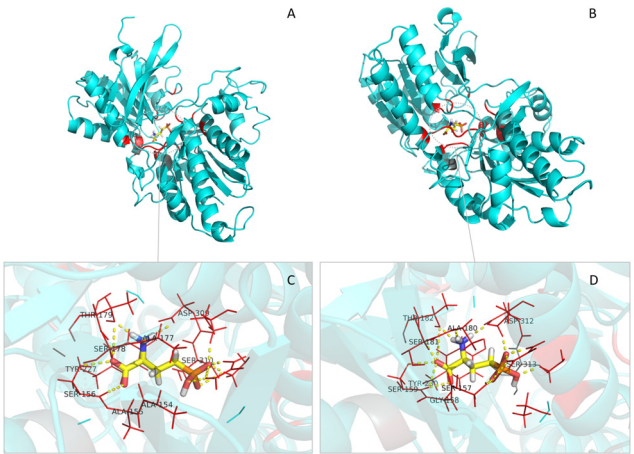

Fig. 6 Interaction between CHEMBL33567 and two receptors. The polar interaction between ligand and binding-pocket residues is shown in yellow dashed lines and ligand atoms are colored by elements. Residues within 5 Å to the ligands are shown in lines. The red color of residues represents strong residue–ligand interaction, grey color represents medium residue–ligand interaction and cyan represents low residue–ligand interaction. (A) Overall view of the ligand–receptor complex of CHEMBL33567 and mGluR8. (B) Overall view of the ligand–receptor complex of CHEMBL 33567 and mGluR4. (C) Detailed interaction between CHEMBL33567 and binding-site residues of mGluR8. (D) Detailed interaction between CHEMBL33567 and binding-site residues of mGluR4.

RMSD value of the mainchain atom coordinate compared to the average coordinate of the mainchain atom during the sampling phase. All functional groups within the three regions shown in Fig. 5 can form H-bonds with surrounding residues. However, at the right side of the binding pocket, the negatively charged functional group of CHEMBL33567, $-HPO_3^-$ has more polar interactions with surrounding residues than that of CHEMBL 575060, $-COO^-$. Overall, there are more H-bonds for mGluR8 than mGluR4 for both ligands, consistent with the observation that both ligands bind more tightly to mGluR8 than to mGluR4. We also observed that CHEMBL33567 forms more H-bonds with the surrounding residues than CHEMBL575060, also consistent with the experimental finding that CHEMBL33567 is more potent than CHEMBL575060.

Besides, we have also compared our findings with the literature.[50] According to the research investigating the structure–activity relationship of ligands serving as agonists and antagonists of mGluRs, the agonists and antagonists identified during *in vitro* tests for mGluR4 all have a structure pattern in accordance with our findings. To summarize their structural feature, favorable ligands are all amino acid analogs. The pseudo side-chains consist of Cα (alpha carbon), Cβ (beta carbon), Cγ (gamma carbon), and the Δ (delta) position either has a $-COO^-$ or a $-HPO_3^-$. As a result, the functional groups at the top, right and left side of the ligand binding pocket tend to interact with surrounding residues. For example, at the left side of the binding pocket, the $-COO^-$ of an amino acid analog can form H-bonds with SER178 (mGluR8)/SER157 (mGluR4). At the top part of the binding pocket, ALA177 (mGluR8)/ALA180 (mGluR4) can form an H-bond with the $-NH_3^+$ functional group of the amino acid analog. The ASP309 (mGluR8)/ASP312 (mGluR4) at the right side of the binding pocket can also have H-bond interactions with the functional group at the Δ (delta) position of the ligand pseudo side-chain.

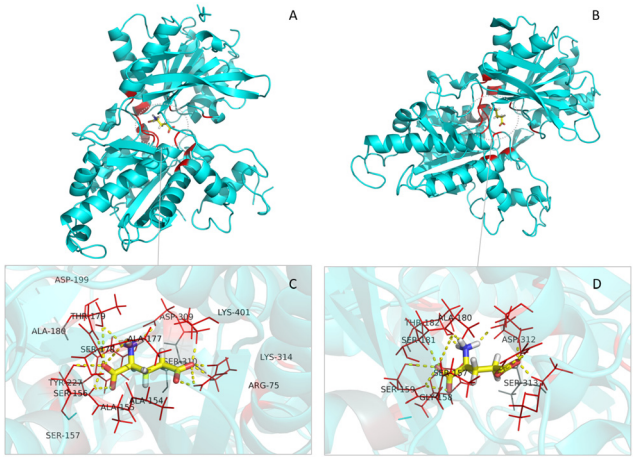

Fig. 7 Interaction between CHEMBL575060 and two receptors. The polar interaction between ligand and binding-pocket residues is shown in yellow dashed lines and ligand atoms are colored by elements. Residues within 5 Å to the ligands are shown in lines. The red color of residues represents strong residue–ligand interactions, the grey color represents medium residue–ligand interaction and cyan represents low residue–ligand interaction. (A) Overall view of the ligand–receptor complex of CHEMBL575060 and mGluR8. (B) Overall view of the ligand–receptor complex of CHEMBL575060 and mGluR4. (C) Detailed interaction between ligand and binding-site residues of mGluR8. (D) Detailed interaction between ligand and binding-site residues of mGluR4.

Though the above preliminary speculation is useful in novel drug development, it is still unclear how to develop highly potent, and selective modulators for mGluR8 or mGluR4. To further understand the mechanisms which govern the binding potency and selectivity between the two receptors, we conducted binding free energy decomposition using MM-GBSA2. Although the correlation between the predicted binding free energies from MM-GBSA5 and the experiment reported K_i values shows the best result under different prediction models, the calculated energies also pose the highest standard errors (SD) (Tables S2–S9, ESI†), and that's the reason we chose the MM-GBSA2 model, the runner-up scoring function in correlation analysis, to conduct the energy decomposition analysis.

According to the MM-PB/GBSA binding free energy calculation results, we selected 7 ligands which are experimentally reported the most active as well as predicted with a high binding affinity for both mGluR8 and mGluR4 for analyzing hotspot residues. For each receptor–ligand complex, 4000 snapshots were collected from the sampling phase during MD simulation to conduct the MM/GBSA free energy decomposition calculation. The mean values of the interaction energy between receptors and ligands were calculated from the snapshots and hotspot residues were identified with the cutoff value of -0.3 kcal mol^{-1}. All the hotspot residues that have ligand–residue interaction energy no larger than -0.3 kcal mol^{-1} are shown in Fig. 8 and 9 for mGluR8 protein and mGluR4 protein, respectively.

From the heatmaps for both receptors, the key residues of mGluR8 and mGluR4 share a high similarity as expected. ARG75 (mGluR8)/ARG78 (mGluR4), SER156 (mGluR8)/SER159 (mGluR4), ASP309 (mGluR8)/ASP312 (mGluR4), LYS314 (mGluR8)/LYS317 (mGLuR4), and LYS401 (mGluR8)/LYS405 (mGluR4) show very strong interaction energies with each ligand, reflected by a darker color. These shared hotspot residues can explain why mGluR8 and mGluR4 proteins share many binding ligands. Besides, among the hotspot residues not recognized by both receptors, ALA154 and ALA155 of mGluR8, and SER157 and GLY158 of mGluR4 show outstanding interactions with ligands, demonstrating that these residues may be the most important hotspot residues responsible for the selectivity between mGluR8 and mGluR4. Therefore, the binding free energy decomposition analysis can quantitively identify hotspot residues that contribute most to the potency and selectivity of ligand binding. The binding profile resulting from MM-GBSA decomposition analysis can guide us to develop potent and selective ligands targeting mGluR4 or mGluR8.

5 The application of homology modeling-docking-MD simulation-binding free energy prediction protocol and machine learning prediction

In this study, we applied a three-step HVS method to screen the active ligand for mGluR4, which does not have a resolved crystal structure, and which has only a limited number of ligands with experimental binding affinities. By comparing the prediction result and the reported experimental ΔG value of ligands ranging from a high binding affinity to low, along with the correlation level reflected by the R-value, we demonstrated that flexible docking and MD simulation followed by MM-PB/GBSA-WSAS analysis can both predict the binding affinity for a ligand, with MD simulation and subsequent binding free energy prediction and decomposition coming up with more precise prediction results. The experimentally reported active ligands can be successfully identified by this hierarchical screening protocol, which demonstrates the practicability of applying HVS in searching for potential hits or leads of mGluR4 through a larger-scale screening study. We are in the process of conducting HVS using druglike screening libraries for the mGluR4 target and the result will be reported elsewhere.

For the three-step HVS method, Glide docking can be performed first to make the preliminary selection of active ligands from an extremely large library which contains even millions of small molecules within days and followed by MD simulation for more accurate calculations of binding free energies for the top hits. The final yielded active ligands with predicted high affinities should be very promising to be developed into drug leads and candidates. Besides, although this study is aimed at developing a virtual screening method for ligands targeting mGluR4, this method may also be applied to study another pair of Group III mGluRs, mGluR6 and mGluR7, for which there is a high homology between them and mGluR6 has no experimental structure available while mGluR7 has two PDB entries (Table S1, ESI†). Furthermore, this modeling protocol, which consists of homology modeling, fast docking simulations, MD simulations for testing ligand–protein binding stability, and endpoint free energy calculations using

Fig. 8 The heatmap of mGluR8 protein. The *Y*-axis labels are the names and ID numbers of key residues. The *X*-axis labels are seven selected ligands and the predicted MM-GBSA2 binding affinities are consistent with experimental results and with low K_i values for mGluR8. The bar on the right is a color map measuring the strength of a ligand–residue interaction.

MM-PB/GBSA-WSAS can be applied to other proteins for which no resolved crystal structures are available.

Molecular docking is an efficient method which can be much quicker but less accurate than MD to predict possible binding poses of a ligand binding to the receptor with docking scores to measure its binding affinity. Unlike MD simulations which study the dynamics of ligand-target interaction in an aqueous solution which mimics the physiological condition of the human body, docking uses only static conformations to predict a ligand's binding affinity to the protein. Literature studies have shown that docking methods can successfully predict near-native binding poses, but the binding affinities predicted by the corresponding docking scores are much less satisfactory.[51–53] However, with the docking poses generated from Glide docking as the starting conformations of the MD processes, the unfavorable ligands will be filtered out through post-MD trajectory analysis and binding free energy calculation. The final simulation result from MD is thus reliable.

IPSF is an advanced technique which can address the heterogeneity issue of protein–ligand binding using a machine learning algorithm. However, its limitation lies in that a large number of active and inactive ligands with measured binding affinities must be known to construct the drug target-specific IPSF. This requirement may limit the usage of IPSF for a new drug target which typically does not have a large number of active and inactive ligands. In this work, we have demonstrated that for a typical drug target like mGluR4 or mGluR8 which has tens of ligands with relatively diverse binding affinities, high-quality target-specific IPSF can be constructed to identify new binders through virtual screenings.

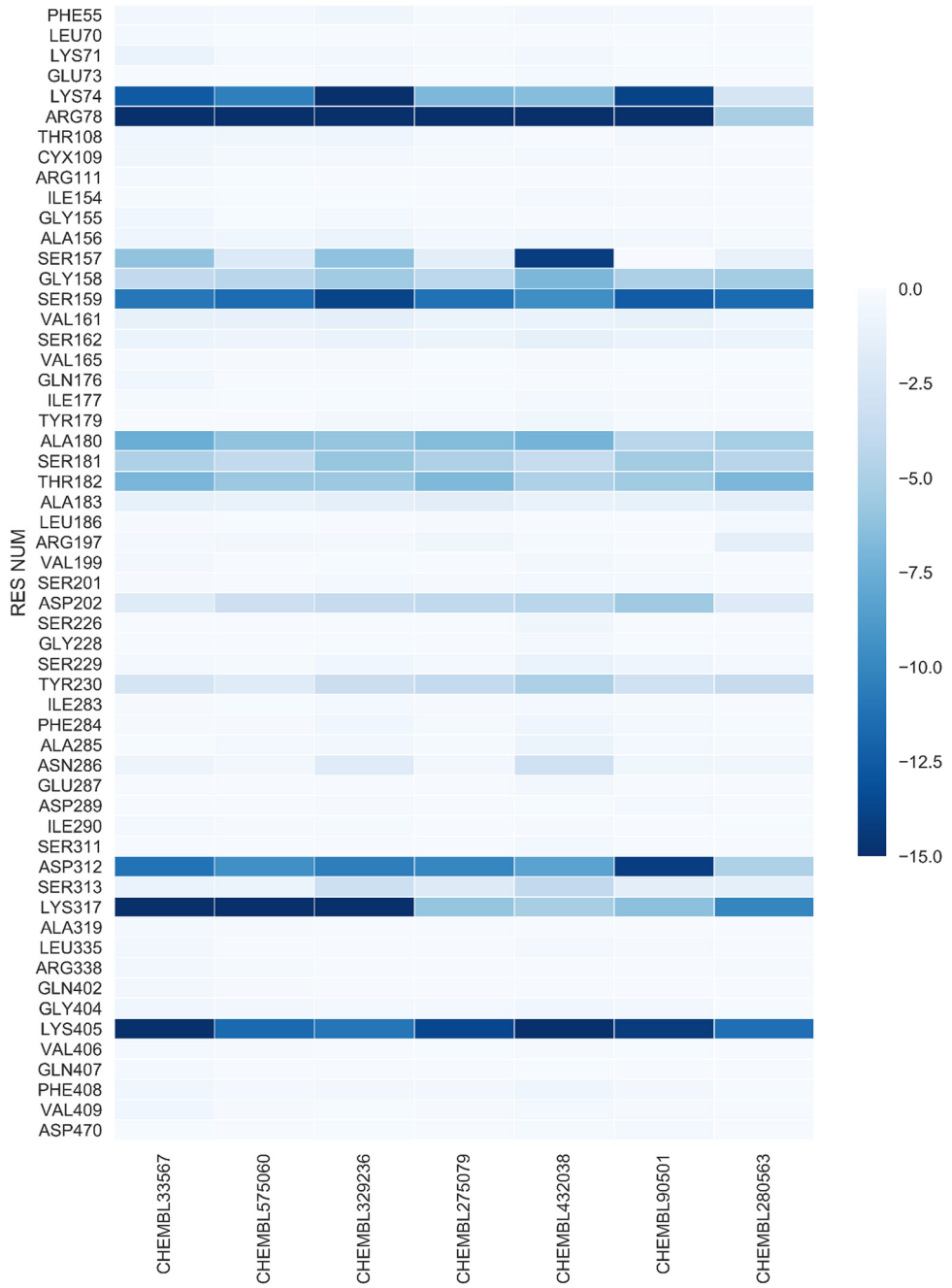

Fig. 9 The heatmap of mGluR4 protein. The *Y*-axis labels are the names and numbers of key residues. The *X*-axis labels are seven selected ligands which the predicted MMGBSA2 binding affinities are consistent with experimental results and with low K_i values for mGluR4. The bar on the right is a color map measuring the strength of a ligand–residue interaction.

After validating IPSF scoring functions in drug lead identification for six drug targets,[20] we evaluated the potential application of IPSF in a typical drug lead optimization project as mGluR4 or mGluR8. Unlike the endpoint methods, the model performance of IPSF models was evaluated using cross-validation RMSE and correlation coefficient R. As expected, the RMSE values, around 1.0 to 1.4 kcal mol^{-1}, are much smaller than those predicted by the endpoint methods. As to the correlation coefficient *R*, the IPSF scoring functions achieved comparable values achieved by the best endpoint method for both mGluRs. Considering the performance of IPSF is not sensitive to the sampling methods,[20] we expect machine learning-based IPSF scoring function can efficiently guide lead optimization without the need of doing long MD simulations to construct a conformation ensemble.

Conclusion

In this study, we tested the practicability of an HVS method on drug lead identification for mGluR8 and mGluR4 proteins, and

the latter does not have a resolved crystal structure so far. The docking and MD simulation screening results of mGluR8 demonstrated the applicability of an HVS method for screening active ligands with regard to a resolved crystal structure of this protein receptor. The application result of this HVS method on the homology model of mGluR4 further demonstrated the practicability of this screening protocol and at the same time validated the homology model we built for mGluR4 using mGluR8 as the template. What's more, with the preliminary screening by molecular docking which can be finished within days and more precise screening by MD simulation, we successfully balanced the computational efficiency and accuracy, which is promising to help improve the success rate and reduce the cost during new drug development. With the initially predicted docking scores for all the ligands in the library and the further prediction of binding free energies for a series of ligands with top-ranked docking scores, active ligands with high binding affinities are prone to be screened out. As such, this VHS protocol which well balances the screening efficiency and accuracy, has high practicability and broad applicability by covering drug targets without solved structures. Moreover, the MM-GBSA decomposition analysis provided guidance on the development of potent and selective ligands targeting a specific receptor, as well as serving as inputs of machine learning to construct IPSF scoring functions to guide drug lead optimization for mGluR8 and mGluR4 drug targets.

Code availability

All the code is available in Amber software.

Conflicts of interest

All the authors declare no conflicts of interest.

Acknowledgements

This work was supported by the funds from the National Science Foundation (1955260) and the National Institutes of Health (R01GM079383). The authors also thank the computing resources provided by the Center for Research Computing (CRC) at the University of Pittsburgh.

References

1 B. A. Wall, S.-S. Shin and S. Chen, Glutamate signaling in human cancers, *Recent advances in the biology therapy and management of melanoma*, 2013, p. 163.
2 A. S. Hauser, M. M. Attwood, M. Rask-Andersen, H. B. Schioth and D. E. Gloriam, Trends in GPCR drug discovery: New agents, targets and indications, *Nat. Rev. Drug Discovery*, 2017, **16**(12), 829–842.
3 S. Rees, D. Morrow and T. Kenakin, GPCR drug discovery through the exploitation of allosteric drug binding sites, *Recept. Channels*, 2002, **8**(5-6), 261–268.
4 J. J. Geurts, G. Wolswijk, L. Bo, S. Redeker, M. Ramkema and D. Troost, *et al.*, Expression patterns of Group III metabotropic glutamate receptors mGluR4 and mGluR8 in multiple sclerosis lesions, *J. Neuroimmunol.*, 2005, **158**(1-2), 182–190.
5 M. Julio-Pieper, P. J. Flor, T. G. Dinan and J. F. Cryan, Exciting times beyond the brain: Metabotropic glutamate receptors in peripheral and non-neural tissues, *Pharmacol. Rev.*, 2011, **63**(1), 35–58.
6 J. Y. Lumeng, B. A. Wall, J. Wangari-Talbot and S. Chen, Metabotropic glutamate receptors in cancer., *Neuropharmacology*, 2017, **115**, 193–202.
7 C. Lüscher and K. M. Huber, Group 1 mGluR-dependent synaptic long-term depression: Mechanisms and implications for circuitry and disease, *Neuron*, 2010, **65**(4), 445–459.
8 F. Bordi and A. Ugolini, Group I metabotropic glutamate receptors: Implications for brain diseases, *Prog. Neurobiol.*, 1999, **59**(1), 55–79.
9 P. J. Conn, Physiological roles and therapeutic potential of metabotropic glutamate receptors, *Ann. N. Y. Acad. Sci.*, 2003, **1003**(1), 12–21.
10 Y. Akiba, C. Watanabe, M. Mizumori and J. D. Kaunitz, Luminal L-glutamate enhances duodenal mucosal defense mechanisms *via* multiple glutamate receptors in rats, *Am. J. Physiol.: Gastrointest. Liver Physiol.*, 2009, **297**(4), G781–G791.
11 H. J. Chang, B. C. Yoo, S. B. Lim, S. Y. Jeong, W. H. Kim and J. G. Park, Metabotropic glutamate receptor 4 expression in colorectal carcinoma and its prognostic significance, *Clin. Cancer Res.*, 2005, **11**(9), 3288–3295.
12 B. C. Yoo, E. Jeon, S. H. Hong, Y. K. Shin, H. J. Chang and J. G. Park, Metabotropic glutamate receptor 4-mediated 5-Fluorouracil resistance in a human colon cancer cell line, *Clin. Cancer Res.*, 2004, **10**(12 Pt 1), 4176–4184.
13 J. D. Panarese, D. W. Engers, Y. J. Wu, J. J. Bronson, J. E. Macor and A. Chun, *et al.*, Discovery of VU2957 (Valiglurax): An mGlu4 positive allosteric modulator evaluated as a preclinical candidate for the treatment of parkinson's disease., *ACS Med. Chem. Lett.*, 2019, **10**(3), 255–260.
14 S. R. Bollinger, D. W. Engers, J. D. Panarese, M. West, J. L. Engers and M. T. Loch, *et al.*, Discovery, structure-activity relationship, and biological characterization of a novel series of 6-((1*H*-pyrazolo[4,3-*b*]pyridin-3-yl)amino)-benzo[*d*]isothiazole-3-carboxamides as positive allosteric modulators of the metabotropic glutamate receptor 4 (mGlu4), *J. Med. Chem.*, 2019, **62**(1), 342–358.
15 D. Charvin, V. Pomel, M. Ortiz, M. Frauli, S. Scheffler and E. Steinberg, *et al.*, Discovery, structure-activity relationship, and antiparkinsonian effect of a potent and brain-penetrant chemical series of positive allosteric modulators of metabotropic glutamate receptor 4, *J. Med. Chem.*, 2017, **60**(20), 8515–8537.
16 R. A. Friesner, R. B. Murphy, M. P. Repasky, L. L. Frye, J. R. Greenwood and T. A. Halgren, *et al.*, Extra precision glide: Docking and scoring incorporating a model of hydrophobic enclosure for protein–ligand complexes, *J. Med. Chem.*, 2006, **49**(21), 6177–6196.

17 J. Wang, P. Morin, W. Wang and P. A. Kollman, Use of MM-PBSA in reproducing the binding free energies to HIV-1 RT of TIBO derivatives and predicting the binding mode to HIV-1 RT of efavirenz by docking and MM-PBSA, *J. Am. Chem. Soc.*, 2001, **123**(22), 5221–5230.
18 J. M. Swanson, R. H. Henchman and J. A. McCammon, Revisiting free energy calculations: A theoretical connection to MM/PBSA and direct calculation of the association free energy, *Biophys J.*, 2004, **86**(1 Pt 1), 67–74.
19 S. Lin, S. Han, X. Cai, Q. Tan, K. Zhou and D. Wang, *et al.*, Structures of Gi-bound metabotropic glutamate receptors mGlu2 and mGlu4., *Nature*, 2021, **594**(7864), 583–588.
20 B. Ji, X. He, J. Zhai, Y. Zhang, V. H. Man and J. Wang, Machine learning on ligand-residue interaction profiles to significantly improve binding affinity prediction, *Briefings Bioinf.*, 2021, **22**(5), bbab054.
21 A. Gaulton, A. Hersey, M. Nowotka, A. P. Bento, J. Chambers and D. Mendez, *et al.*, The ChEMBL database in 2017, *Nucleic Acids Res.*, 2017, **45**(D1), D945–D954.
22 U. Consortium, UniProt: A hub for protein information, *Nucleic Acids Res.*, 2015, **43**(D1), D204–D212.
23 J. Pei, B. H. Kim and N. V. Grishin, PROMALS3D: A tool for multiple protein sequence and structure alignments, *Nucleic Acids Res.*, 2008, **36**(7), 2295–2300.
24 S. K. Burley, H. M. Berman, C. Christie, J. M. Duarte, Z. Feng and J. Westbrook, *et al.*, RCSB protein data bank: Sustaining a living digital data resource that enables breakthroughs in scientific research and biomedical education, *Protein Sci.*, 2018, **27**(1), 316–330.
25 A. Fiser and A. Šali, Modeller: Generation and refinement of homology-based protein structure models, *Methods in enzymology*, Elsevier, 2003, vol. 374, pp. 461–91.
26 B. Webb and A. Sali, Protein structure modeling with MODELLER, *Protein structure prediction*, Springer, 2014, pp. 1–15.
27 M. Y. Shen and A. Sali, Statistical potential for assessment and prediction of protein structures., *Protein Sci.*, 2006, **15**(11), 2507–2524.
28 R. A. Friesner, J. L. Banks, R. B. Murphy, T. A. Halgren, J. J. Klicic and D. T. Mainz, *et al.*, Glide: A new approach for rapid, accurate docking and scoring. 1. Method and assessment of docking accuracy, *J. Med. Chem.*, 2004, **47**(7), 1739–1749.
29 Z. Wang, H. Sun, X. Yao, D. Li, L. Xu and Y. Li, *et al.*, Comprehensive evaluation of ten docking programs on a diverse set of protein–ligand complexes: The prediction accuracy of sampling power and scoring power., *Phys. Chem. Chem. Phys.*, 2016, **18**(18), 12964–12975.
30 L. Schrödinger, *Schrödinger release 2017-2: Maestro*, Schrödinger LLC, New York, 2017, p. 8.
31 W. L. Jorgensen, J. Chandrasekhar, J. D. Madura, R. W. Impey and M. L. Klein, Comparison of simple potential functions for simulating liquid water, *J. Chem. Phys.*, 1983, **79**(2), 926–935.
32 C. I. Bayly, P. Cieplak, W. Cornell and P. A. Kollman, A well-behaved electrostatic potential based method using charge restraints for deriving atomic charges: The RESP model, *J. Phys. Chem.*, 1993, **97**(40), 10269–10280.
33 M. Frisch, G. Trucks, H. Schlegel, G. Scuseria, M. Robb and J. Cheeseman, *et al.*, *Gaussian 16, revision B. 01*, Wallingford, CT, 2016, Google Scholar There is no corresponding record for this reference.
34 J. Wang, R. M. Wolf, J. W. Caldwell, P. A. Kollman and D. A. Case, Development and testing of a general amber force field, *J. Comput. Chem.*, 2004, **25**(9), 1157–1174.
35 T. Darden, R. Duke, D. Ghoreishi, M. Gilson, H. Gohlke and A. Goetz, *et al.*, *AMBER 2018*, University of California, San Francisco, 2018.
36 J. Wang, W. Wang, P. A. Kollman and D. A. Case, Automatic atom type and bond type perception in molecular mechanical calculations, *J. Mol. Graphics Modell.*, 2006, **25**(2), 247–260.
37 J. A. Maier, C. Martinez, K. Kasavajhala, L. Wickstrom, K. E. Hauser and C. Simmerling, ff14SB: Improving the accuracy of protein side chain and backbone parameters from ff99SB, *J. Chem. Theory Comput.*, 2015, **11**(8), 3696–3713.
38 H. J. Berendsen, J. V. Postma, W. F. van Gunsteren, A. DiNola and J. R. Haak, Molecular dynamics with coupling to an external bath, *J. Chem. Phys.*, 1984, **81**(8), 3684–3690.
39 R. J. Loncharich, B. R. Brooks and R. W. Pastor, Langevin dynamics of peptides: The frictional dependence of isomerization rates of *N*-acetylalanyl-*N*′-methylamide, *Biopolymers*, 1992, **32**(5), 523–535.
40 J. Wang, T. Hou and X. Xu, Recent advances in free energy calculations with a combination of molecular mechanics and continuum models, *Curr. Comput.-Aided Drug Des.*, 2006, **2**(3), 287–306.
41 T. Hou, J. Wang, Y. Li and W. Wang, Assessing the performance of the MM/PBSA and MM/GBSA methods. 1. The accuracy of binding free energy calculations based on molecular dynamics simulations, *J. Chem. Inf. Model.*, 2011, **51**(1), 69–82.
42 T. Hou, J. Wang, Y. Li and W. Wang, Assessing the performance of the MM/PBSA and MM/GBSA methods: II. The accuracy of ranking poses generated from docking, *J. Comput. Chem.*, 2011, **32**(5), 866.
43 J. Wang and T. Hou, Develop and test a solvent accessible surface area-based model in conformational entropy calculations, *J. Chem. Inf. Model.*, 2012, **52**(5), 1199–1212.
44 E. Wang, H. Liu, J. Wang, G. Weng, H. Sun and Z. Wang, *et al.*, Development and evaluation of MM/GBSA based on a variable dielectric GB model for predicting protein–ligand binding affinities, *J. Chem. Inf. Model.*, 2020, **60**(11), 5353–5365.
45 T. Hou, J. Wang, Y. Li and W. Wang, Assessing the performance of the molecular mechanics/Poisson Boltzmann surface area and molecular mechanics/generalized born surface area methods. II. The accuracy of ranking poses generated from docking, *J. Comput. Chem.*, 2011, **32**(5), 866–877.
46 F. Chen, H. Sun, J. Wang, F. Zhu, H. Liu and Z. Wang, *et al.*, Assessing the performance of MM/PBSA and MM/GBSA

methods. 8. Predicting binding free energies and poses of protein-RNA complexes, *RNA*, 2018, **24**(9), 1183–1194.

47 I. Massova and P. A. Kollman, Combined molecular mechanical and continuum solvent approach (MM-PBSA/GBSA) to predict ligand binding, *Perspect. Drug Discovery Des.*, 2000, **18**(1), 113–135.

48 G. D. Hawkins, C. J. Cramer and D. G. Truhlar, Parametrized models of aqueous free energies of solvation based on pairwise descreening of solute atomic charges from a dielectric medium, *J. Phys. Chem.*, 1996, **100**(51), 19824–19839.

49 A. Onufriev, D. Bashford and D. A. Case, Exploring protein native states and large-scale conformational changes with a modified generalized born model, *Proteins*, 2004, **55**(2), 383–394.

50 N. Sekiyama, Y. Hayashi, S. Nakanishi, D. Jane, H. W. Tse and E. Birse, *et al.*, Structure-activity relationships of new agonists and antagonists of different metabotropic glutamate receptor subtypes, *Br. J. Pharmacol.*, 1996, **117**(7), 1493–1503.

51 R. A. Friesner, J. L. Banks, R. B. Murphy, T. A. Halgren, J. J. Klicic and D. T. Mainz, *et al.*, Glide: A new approach for rapid, accurate docking and scoring. 1. Method and assessment of docking accuracy, *J. Med. Chem.*, 2004, **47**(7), 1739–1749.

52 S. Gathiaka, S. Liu, M. Chiu, H. Yang, J. A. Stuckey and Y. N. Kang, *et al.*, D3R grand challenge 2015: Evaluation of protein–ligand pose and affinity predictions, *J. Comput.-Aided Mol. Des.*, 2016, **30**(9), 651–668.

53 Z. Gaieb, S. Liu, S. Gathiaka, M. Chiu, H. Yang and C. Shao, *et al.*, D3R grand challenge 2: Blind prediction of protein–ligand poses, affinity rankings, and relative binding free energies, *J. Comput.-Aided Mol. Des.*, 2018, **32**(1), 1–20.